Supplementary Information:

Mechanical properties of the rocky interiors of icy moons

C. Seltzer, H.O. Ghaffari, M. Peč

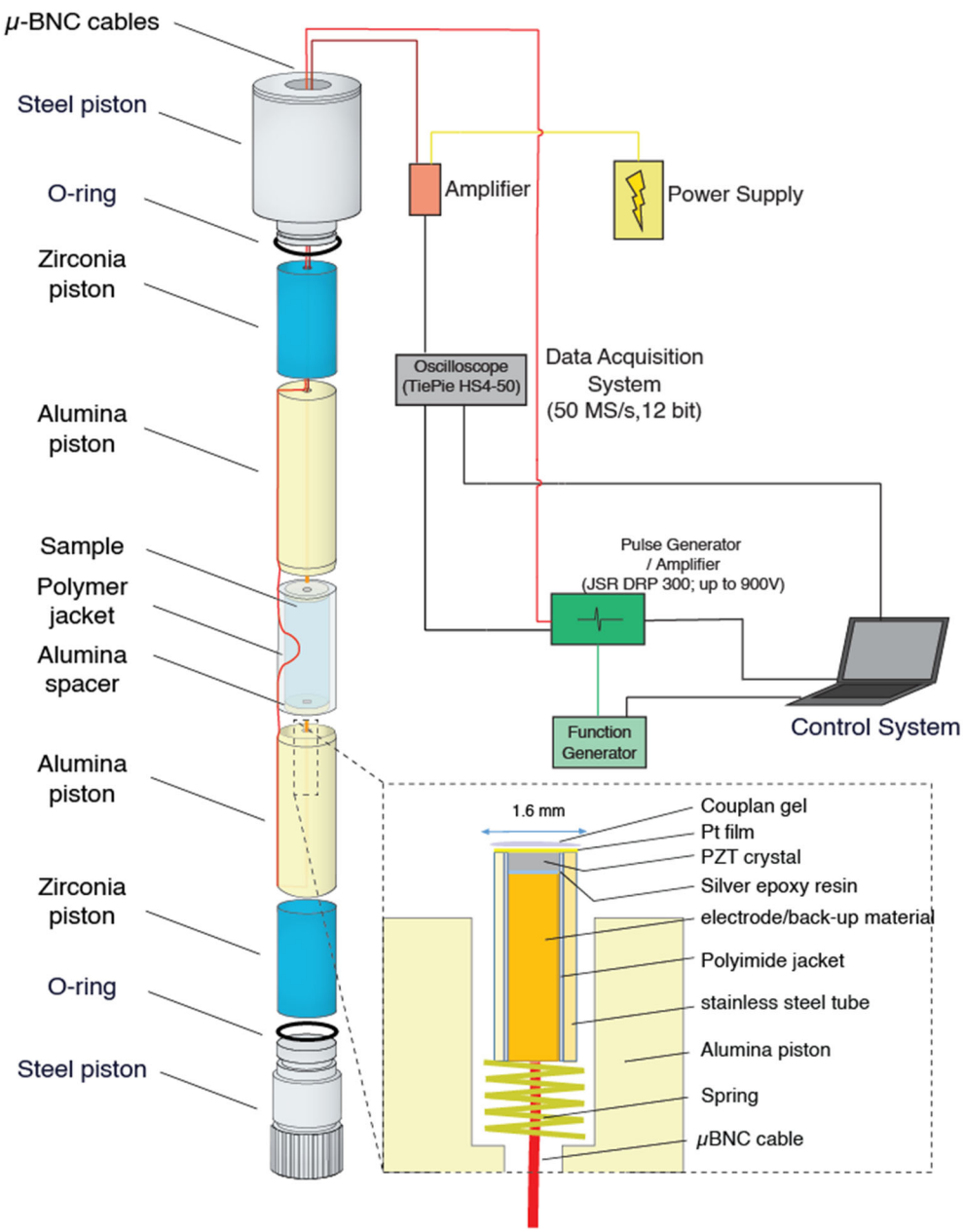

Figure S1: Schematic of our sample setup and ultrasonic instrumentation method.

All experiments were conducted in a Paterson gas medium deformation apparatus, PI-5, in the Rock Deformation Laboratory at MIT. Two custom-made miniature piezo-sensors with stainless steel jacket were threaded through the central hole in the pistons, most commonly used for thermocouples, and mechanically coupled with meteorite sample using springs, as shown in inset. The response of sensors was evaluated before, during and after the tests (using pulse-echo method) to verify the sensors were not lost or weakened by spring-loading process. Signals passed through μ-BMC wires, an amplifier set to amplify signals at 60 dB, and were recorded in a TiePie HS4-50 oscilloscope.

Table T1: experimental parameters for each test.

	Max Pc (MPa)	initial length (mm)	diameter (mm)	max diff. stress (MPa)	dx rate (mm/min)	strain rate (s^{-1})	T (K)	AEs
001_CS_PI	54	11.73	6.75	428	0.072	1E-05	295	yes
009_CS_PI	28	10.05	6.77	193	0.029	5E-05	295	no
010_CS_PI	16	10.55	6.76	138	0.032	5E-05	295	no
012_CS_PI	72	11.5	6.75	289	0.035	5E-05	295	yes
013_CS_PI	42	9.34	6.75	214	0.028	5E-05	295	yes
015_CS_PI	100	8.93	6.74	265	0.027	5E-05	295	yes
017_CS_PI	20	7.82	6.66	50	0.023	5E-05	295	yes
019_CS_PI	40	6.72	6.72	72	0.023	5E-05	295	no
032_CS_PI	45	7.3	6.25	265	0.022	5E-05	295	yes
033_CS_PI	50	7.3	6.75	311	0.022	5E-05	295	yes
037_CS_PI	47	7.29	6.66	268	0.022	5E-05	295	yes

Table T1. Each test is recorded by name in the farthest left column. Pc = confining pressure, dx rate = displacement rate, T = temperature. AEs column indicates whether sensors were in place and able to record acoustic emissions.

On the calibration of amplifiers and piezoelectric sensors:

The response of amplifiers at 60 dB was tested at room conditions by sending a sinusoidal pulse with different frequencies and amplitudes through the same length of BNC cables used in the real set-up of our tests. The response of the amplifier is flat amplification of ~57 dB up to 1.5 MHz, after which there was an exponential decreasing of amplification from 57 dB to 35 dB at frequencies up to ~15 MHz. The majority of recorded signals were in the frequency range ~50 kHz to 2 MHz. Note that the employed amplifiers did not distort or change the shape of the sine waves for excited signals below 500 mV, and correctly transferred the frequency of the input waves.

To calibrate the response of the sensor, we used a 3D laser Doppler vibrometer (LDV) which can measure the vibration rates in three perpendicular directions (Ghaffari et al., 2021) and is sensitive to signals from 5kHz to ~300kHz. We calibrated these sensors within a frequency range <400kHz, in order to set a lower limit in measuring velocities and displacements. The sensor (instrument) response can be isolated once we identify the amplitude-power of a reference sensor or probe ($P_{LDV}(\omega)$) and of a test sensor ($P_{PZT}(\omega)$) for the same vibration. Here, the source could be a fixed source generated by a vibrating sensor due to sinusoidal waveforms, or an impulse-electrical signals generating a train of waves with different frequencies in the source sensor. The instrument response or transform function in power-frequency domain is defined such that $I(\omega) = \frac{P_{PZT}(\omega)}{P_{LDV}(\omega)}$. For an ideal sensor, I(ω)=1. However,

here we have partial overlap of frequencies between the two sensors, so our instrument response function is valid for the domain from 40kHz-300kHz.

We calibrated the needle (miniature) sensors used in our experiments in two different set-ups: **I)** in the first set-up, a pulsing sensor was triggered with a sweep mode of sinusoidal wave pulses at frequencies of 10 kHz to 5 MHz. The receiver sensor receives the signal directly. A thin film of mica is used to prevent electrical noise and interference. The pulsing transducer's pressure field (radiation field) is characterized independently with pulse-echo (in air) method, where the sensor receives a short ~100 ns electrical pulse and the vibration of the sensor is recorded at 0 dB amplification. The energy input of electrical pulse is set to be equal with amplitude of pulses in the main set-up. We use spectral analysis to obtain amplitudes for each frequency domain (at bin size of 10 kHz), then integrated to define total power at each frequency, P(ω). We evaluated the receiver sensor as the main sensing element by its sensitivity (loop gain, insertion loss) parameter, $S(dB) = 20 \log (V_x/ V_0)$, where V_x is the amplitude of the received signal in volts at a given frequency and V_0 is the amplitude of transducer excitation in volts at the same frequency. In Figure S2 we show the S-parameter. An almost flat response relative to the source sensor is achieved in the frequency range of 0.35-1.5MHz

II) We also calibrated our sensors with an on-table test (**Figure S2**) in which we used a cylindrical rock sample and two sensors spring-loaded to end surfaces of the sample. One sensor served as a source, pulsing signals through the sample which were received at the other end, where laser beams of LDV measured the velocity components. To compare the response of the receiver sensor with the laser measurements, we calculated an overlapped (80%) 2,048-point fast Fourier transform to calculate the power of the signal. Next, we calculated the average of the power of the waveform over a frequency range from 50 kHz to 300kHz($<P>_\omega$) (**Figure S2e**). $<P(t)>_\omega$ has a peak-like form and includes a fast-rising phase which is followed by a fast drop (**Figure S2c**). Response of the sensor encoded in $<P>_\omega$ closely matches with the z-component of slip velocity profile measured by laser beams. Similarity of out of plane velocity profile to $<P(t)>_\omega$ (Figure 3e) yields a lower bound estimate of displacement:

Considering an approximation for particle velocity: $|v(t)| \equiv < P(t) >_\omega$, we find a total integrated displacement $d(t) \equiv \int < P(t) >_\omega \, dt$ (**Figure S2f**). For the illustrated case in **Figure S2**, the maximum displacement in the sensor location during ~30 μs rise-time of the slip rate is ~1.5 nm. In **Figure S3**, we show this analysis applied to a sample waveform recorded during deformation.

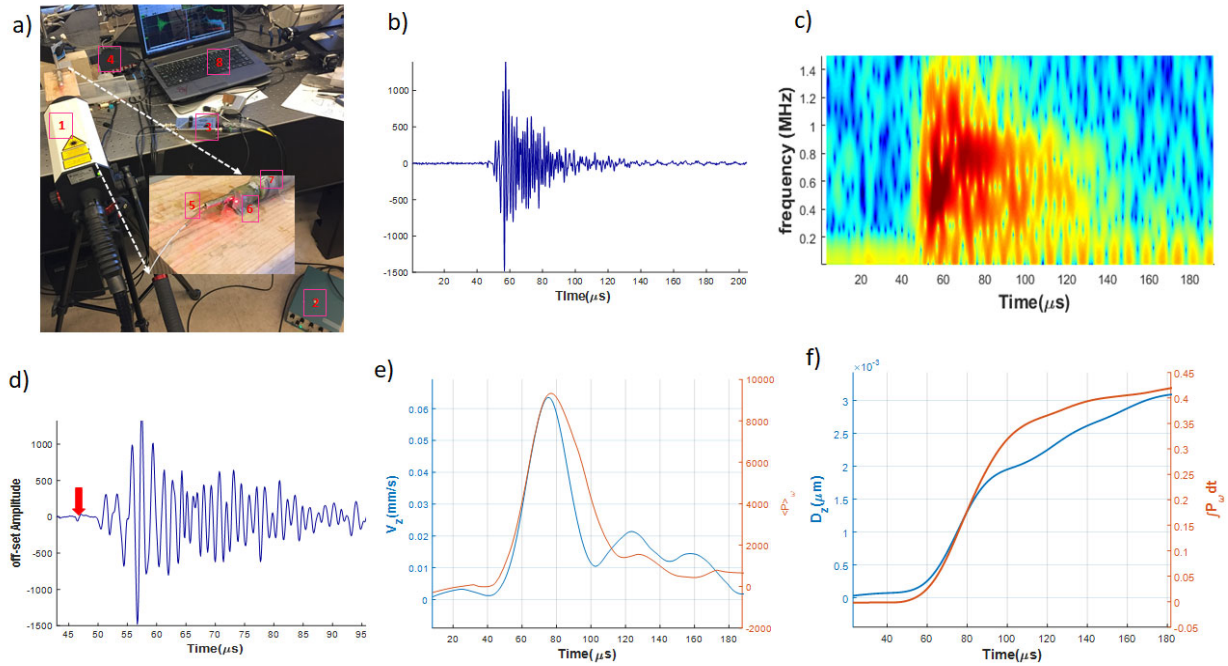

Figure S2. Calibration of the sensors at room conditions with a 3-D laser Doppler vibrometer for signals in the range of 1 kHz < ω <300 kHz. We used a needle piezo-sensor in contact with a rock sample as the receiver and another sensor as the source. The laser beam is placed in vicinity of the receiver sensor that is amplified at 60 dB, and records vibration rates of the rock sample surface in three perpendicular directions. The out of plane component (z- or dilatational component) is obtained and compared with mean of the magnitudes of FT terms over a certain frequency domain $\langle P \rangle_\omega$.

a) Tabletop setup for laser calibration.
b) Full waveform response to laser pulse
c) Frequency-power spectrum for waveform response
d) Truncated waveform, with red arrow indicating arrival time
e) response of the sensor represented with mean power of the signal on the interest frequency domain $\langle P \rangle_\omega$, plotted alongside the slip velocity for displacement recorded within the waveform.
f) total displacement and total power during waveform

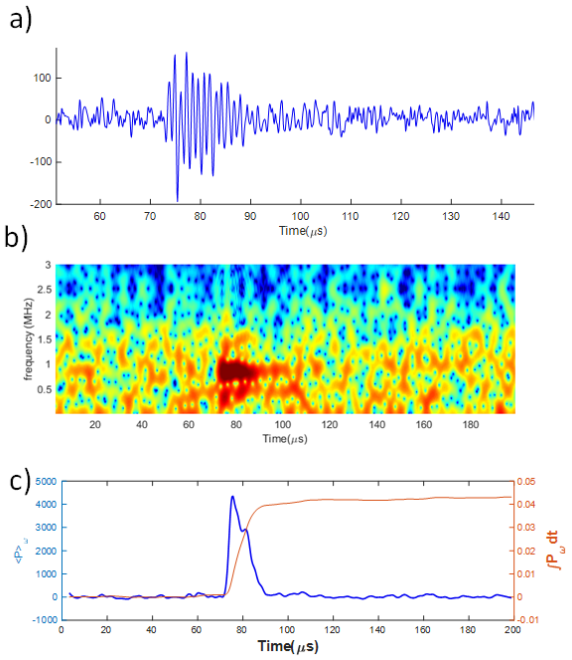

Figure S3. Spectral analysis of a waveform emitted during deformation under confining pressure of 100 MPa. a) Acoustic waveform, b) frequency-power spectrum, c) total power released.

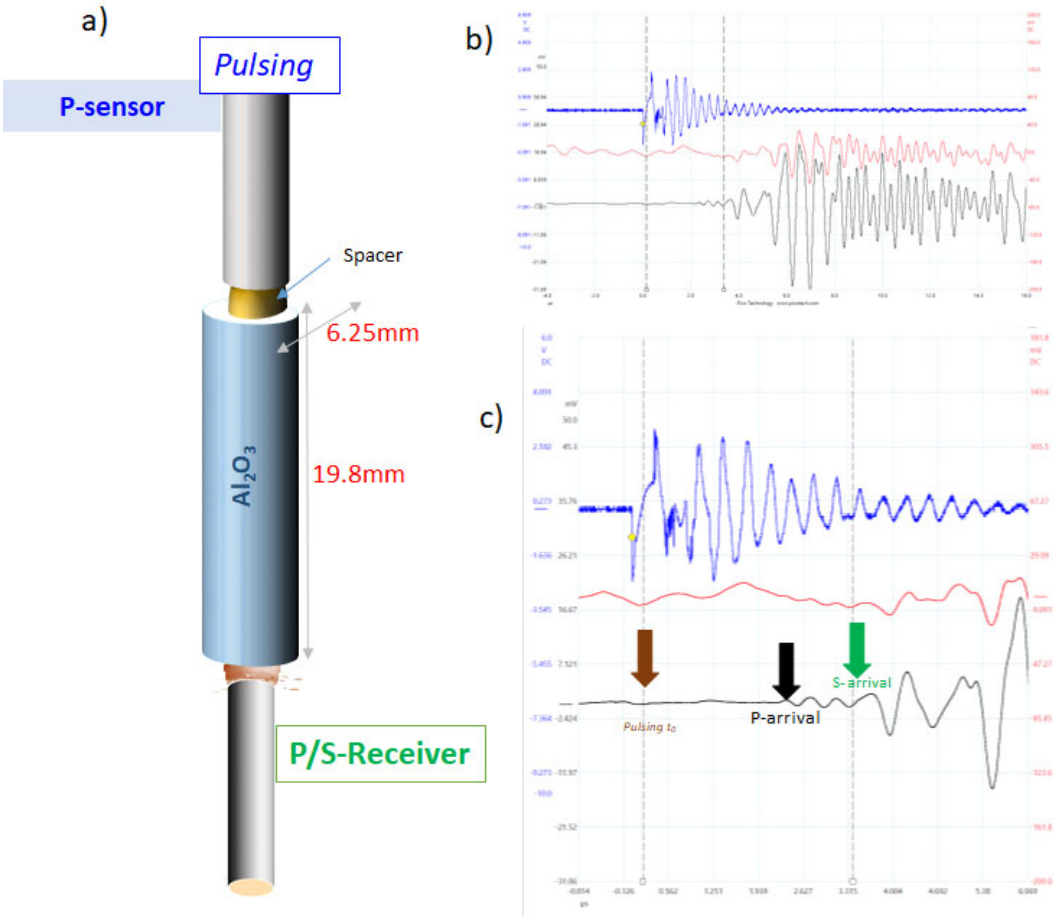

Figure S4: Pulsing-receiving sensor setup and calibration.

a) We used a rod of alumina to calibrate waveforms before picking from real tests. b) Sample waveform from calibration. Alumina sound velocities under room conditions for P and S waves are 9.9 and 6.5 km/s, respectively. c) Wave picking from calibration. There is a weak P arrival, but strong S arrival.

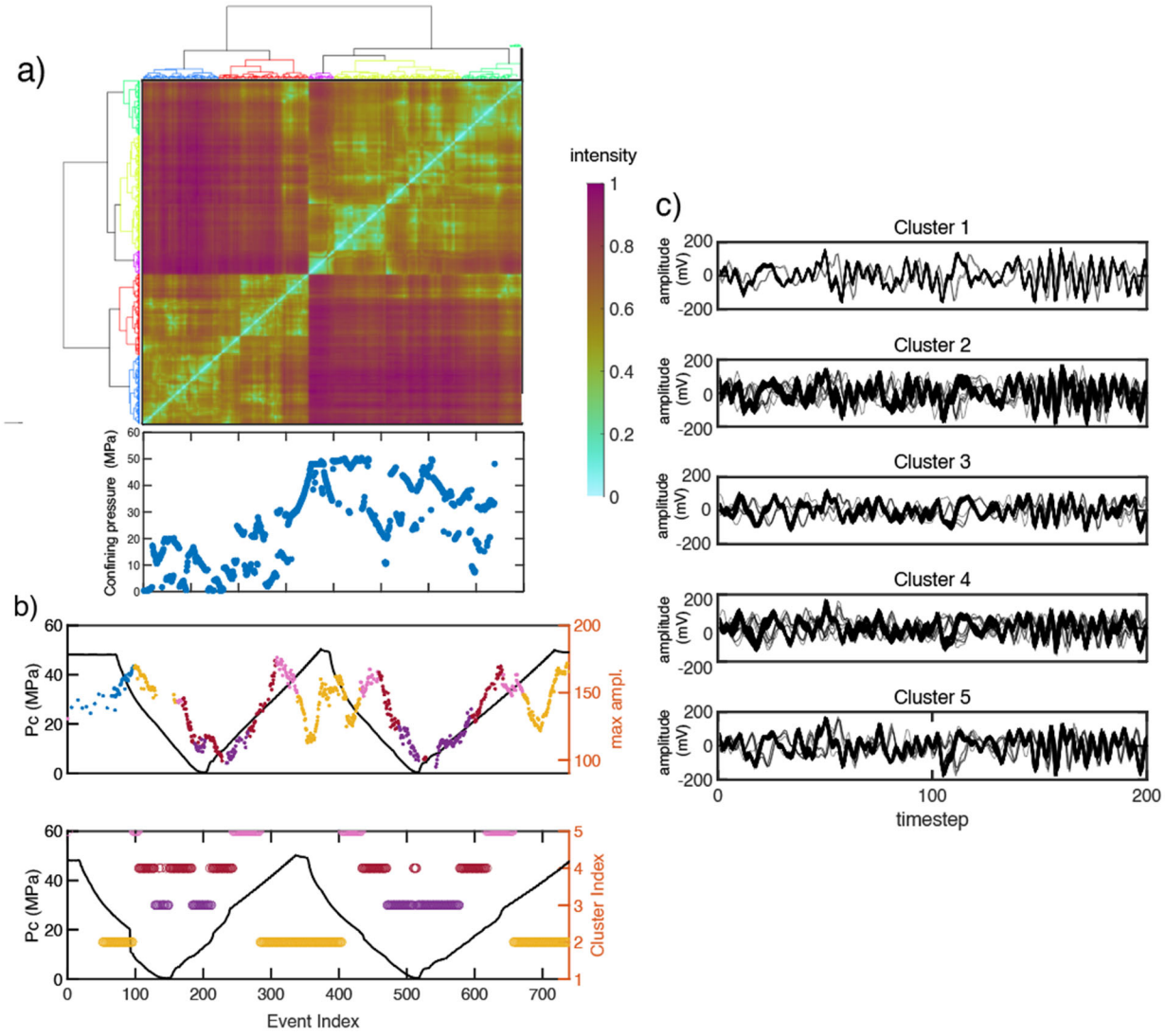

Figure S5: Clustering of active ultrasonic pulses during two cycles of pressurization-depressurization up to 50 MPa Pc. We used a dynamic time warping (DTW) metric to compare 'distance' of waves and used hierarchical clustering. a) Clustergram, accompanied with confining pressure graph, b) Plot of max amplitude and cluster index overlying confining pressure graph, c) waveforms from each cluster.

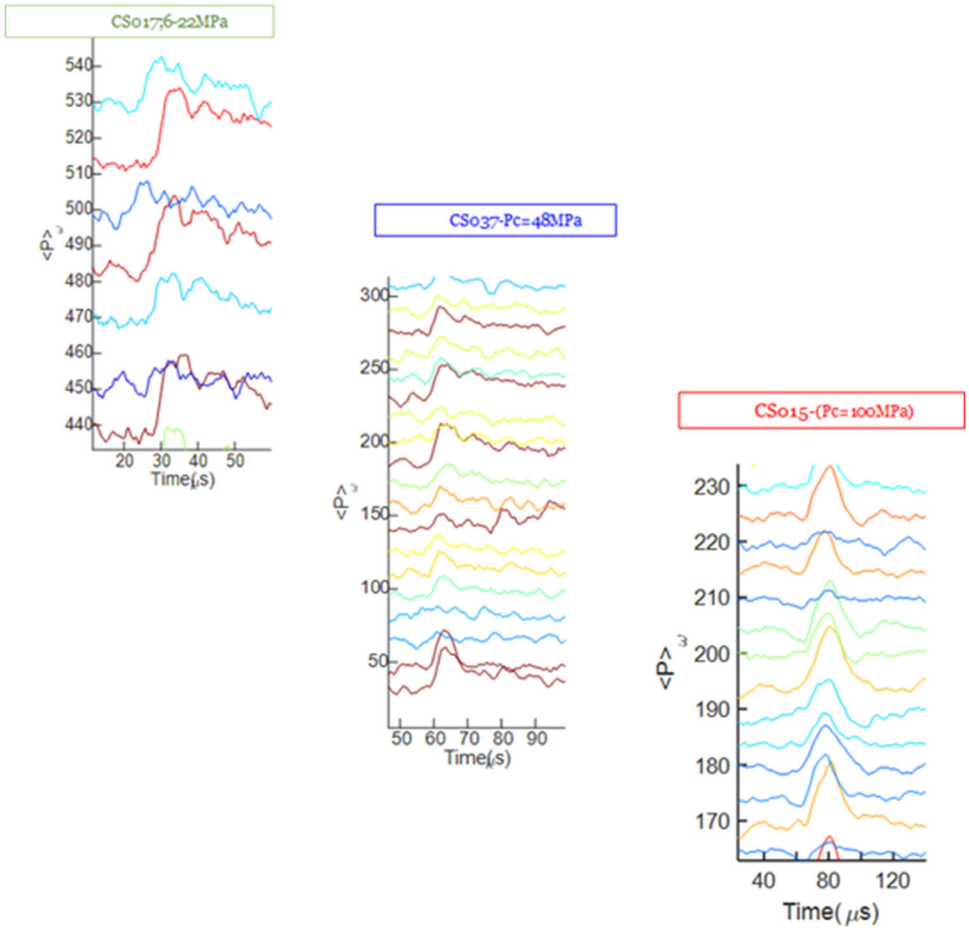

Figure S6: <P(t)> parameter for AEs at three different confining pressures. <P(t)> scales with particle velocity at the sensor location. As pressure increases the signal's skewness change and approaches ~symmetric pulse.